Aluminum-enhanced alkali diffusion from float glass to PVD-sputtered silica thin films

Jean-Thomas Fonné, Ekaterina Burov, Emmanuelle Gouillart, Sergey Grachev, Hervé Montigaud, Damien Vandembroucq

Aluminum-enhanced alkali diffusion from float glass to PVD-sputtered silica thin films

Jean-Thomas Fonné*, Ekaterina Burov*, Emmanuelle Gouillart*, Sergey Grachev*, Hervé Montigaud*

Surface du Verre et Interfaces, UMR 125 CNRS/Saint-Gobain, 93303 Aubervilliers, France

Damien Vandembroucq*

Laboratoire PMMH, UMR 7636 CNRS/ESPCI/Univ. Paris 6 UPMC/Univ. Paris 7 Diderot, 10 rue Vauquelin, 75231 Paris cedex 05, France

Abstract

Interdiffusion processes between aluminum enriched PVD-sputtered silica thin films and industrial float soda-lime silicate glass substrates are quantitatively studied using SIMS analysis. Heat treatments are performed at temperatures close or above the glass transition temperature of the float glass. Aluminum doping of the film is shown to strongly increase the migration of alkali from the glass substrate to the silica thin film. In particular the final alkali content in the film exhibits a linear scaling with the aluminum concentration. An interdiffusion process is evidenced between bulk alkali ions and protons originating from a significant water content in the as-deposited silica film. Experimental measurements of sodium concentration are shown to be consistent with a simple thermodynamic model based on the equilibration of the activity of sodium between the film and the glass substrate.

Keywords: Silica thin film, Barrier layer, Alkali-ions migration, Interface diffusion

1. Introduction

Industrial glasses coated with thin films are often subjected to thermal treatments, in the framework of a forming process, or in order to enhance specific properties of the glazing, or to improve the mechanical properties of glass. At high temperature close or above the glass temperature of the substrate, several species diffuse from the substrate to the thin films. For soda-lime float glass, the diffusion of sodium or other alkali ions is the most significant effect. Alkali diffusion is beneficial for a minority of active layers, such as $CuGaSe_2$ thin film for solar cells, in which controlled diffusion of sodium and potassium has been shown [1] to enhance energy conversion. However, sodium alters the electrical properties of most active layers used in solar cells [2, 3, 4, 5], with dramatic effects such as electrical shunting caused by the widening of grain boundaries [6]. The diffusion of sodium also decreases the mechanical or electrical properties of low-emissivity coatings [7, 8] used in the building and automotive industry, or of transparent conducting oxide layers used in displays [9].

In order to limit the diffusion of alkali from the glass substrate to the active layers, barrier layers are deposited on the glass surface [2]. Alkali diffusion through a barrier layer has been studied for a variety of compositions, such as silicon nitride [10], silica, alumina [11, 12] or ceria [13], and for different deposition processes such as chemical vapor deposition (CVD) [14, 15], physical vapor deposition (PVD) [7, 8], or sol-gel coating [16, 17]. One of the most common compositions of barrier layers is silica, which is usually doped with aluminum in PVD coaters in order to increase the deposition rate [18]. For non-doped silica thin films, Araujo et al. [19] showed that the chemical potential of sodium in the substrate could be used to predict whether sodium would diffuse from the substrate to the silica layer, or in the other direction in the case of alumina- or boron-rich substrate compositions.

*corresponding author: jean-thomas.fonne@saint-gobain.com / +33 (0)1 48 39 85 56

Table 1: Composition (in weight percent) of the soda-lime glass substrates.

oxides	weight %
SiO_2	73.0
Na_2O	13.5
CaO	10.0
MgO	2.5
Al_2O_3	0.5
K_2O	0.1
Other elements	< 0.4

Little experimental data exist on the influence of aluminum on alkali diffusion in silica thin films. Nevertheless, the structure and transport properties of bulk aluminosilicate glasses and melts have been studied extensively in the geochemistry community [20, 21, 22, 23, 24]. In particular, the structural role of sodium changes progressively from network modifier to charge compensator of Al^{3+} when alumina is added to a silicate melt [25, 21, 26, 27, 28]. Therefore, adding aluminum to a sodium silicate melt with a fixed Na/Si ratio increases its viscosity, since less sodium is available to depolymerize the silica network [28, 29].

In this work, we study the influence of the aluminum content in silica thin layers on alkali migration at temperatures close to the glass transition of the glass substrate. In particular, our aim is to identify and characterize the diffusion mechanisms at play at the interface between the glass substrate and the PVD-sputtered silica thin films. Using Secondary Ion Mass Spectroscopy (SIMS), we study experimentally alkali migration at 650°C from soda-lime float glass to PVD-sputtered alumina-doped silica layers with different values of aluminum doping. Our experimental results are compared with thermodynamic predictions.

2. Materials and methods

2.1. Glass substrates

Commercial flat soda-lime glass (Saint-Gobain Planiclear®) with a thickness of 2 mm was used as substrate. Its composition is given in Table 1. Samples were prepared, cleaned with RBS^{TM} detergent and rinsed with deionized water before thin film deposition.

2.2. Silica thin films deposition

Pure and aluminum-doped silica layers were deposited by Physical Vapor Deposition (PVD) by cathodic magnetron sputtering at room temperature. Si and Si:Al (8% in weight) targets were used for silica thin films deposition under reactive atmosphere at 2 μbar in Ar/O_2 plasma. Silica layers containing 0% and $\sim 4\%$ (in weight) of Al_2O_3 were obtained by using a single target and SiO_2 thin films with 0.2% to 1% (in weight) of Al_2O_3 were obtained by co-sputtering with the two targets. Therefore, various silica samples with Al_2O_3 concentrations between 0.0 and 4% in weight (corresponding to 0.0 to 2.4% in moles) have been elaborated for this study.

The thickness of the films was measured with surface profilometry (DektakXT, Brucker) or atomic force microscopy (Icon, Brucker). Results for silica layers with thicknesses between 100 nm to 250 nm are presented here. Several deposition chambers were used for this work depending on the size of the samples and the configuration needed (sputtering or co-sputtering).

2.3. Thermal treatments

After deposition on glass, silica thin films were annealed in air at 650°C in an electrical furnace. This temperature is in the range of temperatures used industrially for glass tempering or shaping. One should note that it is higher than the glass-transition temperature (Tg) of the substrate ($\sim$ 550°C). Annealing durations between 5 min and 16 hours were used at this temperature. Samples were directly placed in the furnace prepared at 650°C and quenched in air at the end of the thermal treatment.

2.4. Silica thin films characterization

Quantification of the silica layer was first performed by EPMA (Electron Probe MicroAnalysis) for one thick layer. The measurements were carried out on an SXFive apparatus (CAMECA, France), on samples coated with a thin carbon layer to reduce charging effects. The electrons energies were 5, 10, and 15 keV and the current was 15 nA in order to avoid any sodium diffusion during the acquisition applied on an area of 2 x 40 μm. The X-rays line selected were the following: Na Kα, Si Kα, Al Kα and O Kα. Due to the larger probed depth (> 1 μm) of the technique compared to layer thickness (250 nm), modeling was performed using Stratagem software (SAMX, France). The latter

Table 2: Concentrations (in weight %) of SiO_2, Na_2O and Al_2O_3 in a 250 nm thick silica thin film deposited on glass after 1h at 650°C, measured on the same sample by SIMS (in the central zone), EPMA and XPS.

(weight %)	SiO_2	Na_2O	Al_2O_3	Na/Al (atomic)
SIMS	92.4	3.7	3.9	1.6
XPS	90.8	4.5	4.7	1.6
EPMA	89.9	5.2	4.8	1.8

takes into account the in-depth distribution of the ionization function (called phi(roz)) and based on the XPP model which is well adapted for stratified samples [30]. Quantification by EPMA is given in Table 2.

Furthermore, layer composition for the same sample was estimated by X-ray Photoelectron Spectroscopy (XPS). The analyses were performed on a NOVA system (Kratos-GB) equipped with a monochromatic Al Kα X-ray source, operating at 225W. The collection angle was set at 0° (normal detection) in order to maximize the probe depth (to 5nm in case of such silica-rich material). Results obtained are also given in Table 2.

Since EPMA results consider that the layer composition is homogeneous and XPS only probes the layer surface, SIMS depth profiles were carried out for depth-resolved measurements of the composition. Measurements on as-deposited and annealed silica layers were performed on a TOF.SIMS 5 (ION-TOF GmbH, Münster, Germany). The primary ions Bi^+, accelerated at 30 kV were generated by a LMIG (Liquid Metal Ion Gun) operating in high-current bunched mode with a beam current of 3 pA at 16 kHz. The scanned area of 50 x 50 μm^2 was centered in the middle of the 200 x 200 μm^2 sputter area performed by the DSC (Dual Source Column) source generating Cs^+. The sputter beam energy was 2 keV and the applied current was 150 nA. A usual methodology for non-conductive samples was applied: an electron flood gun was used (E $\sim$ 21 eV) in order to reduce charging effects during the acquisition in non-interlaced mode (1s sputtering, 0.5s pause, 2.5s acquisition)[31].

An example of typical SIMS depth profile is given in Fig. 1. It is generated by the collection of the positive ions coming from the main isotopes elements present within the glass substrate and the layer (i.e.: $^1H^+$, $^{30}Si^+$, $^{23}Na^+$, $^{40}Ca^+$, $^{24}Mg^+$, $^{39}K^+$, $^{27}Al^+$, $^{120}Sn^+$). Cs was selected as abrasive species because it induces less artifacts due to alkali-ions migration during depth profiling [32, 33]. Only monoatomic ions (as opposed to polyatomic clusters) were followed to generate the composition depth profiles, in order to increase the sensitivity within the silica layer [34]. SIMS values at the extreme surface are affected by transitory effects and should not be interpreted [35].

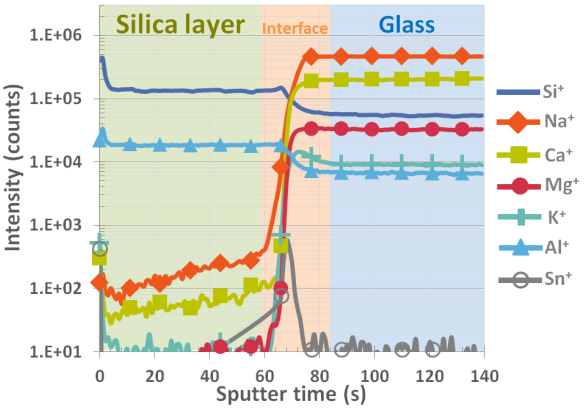

Figure 1: Example of a SIMS depth profile (before calibration) of a silica thin film doped with 0.9-wt% Al_2O_3 as-deposited on glass.

Depth calibration was obtained from stylus profilometry (Dektak XT, Bruker) performed on two different SIMS craters. The first one stopped at the glass/layer interface determined by the maximum of $^{120}Sn^+$ signal. Indeed, tin condensates on the atmospheric side of glass during the floating process (see Fig. 1). We assume that tin is totally oxidized after annealing into Sn^{4+}, which has a negligible mobility [36]. Typical values of the sputtering rate inside the silica layer were between 1.2 and 1.5 nm/s depending on (i) the amount of aluminum, (ii) the deposition conditions and (iii) the thermal treatment. The second crater was stopped deeper in the substrate in order to estimate the sputtering rate for the glass substrate (approximately 1.2 nm/s).

For quantitative depth profiling with SIMS (except for hydrogen), the use of relative sensitivity factors (RSF) is necessary for the conversion of intensities into concentrations [37, 14]. The secondary ion yields of SIMS can be strongly dependent on the composition of the matrix. However, according to the author's experience, we made the assumption that matrix effects are comparable in the dense silica thin films and the soda-lime glass substrate. Therefore the determination of relative sensitivity factors has been made from the compo-

sition of the glass substrate measured by wet chemistry (cf Table 1). Results of the average values of SiO_2, Na_2O and Al_2O_3 content over a central zone (in order to avoid SIMS artifacts) are given in Table 2. Values obtained with these three techniques converge with differences less than ±20%. Consequently, our assumption for SIMS quantification appears to be relevant.

Finally, hydrogen amount was evaluated by Elastic Recoil Detection Analysis (ERDA). The experiment was carried out on the 2.1MeV Van-der-Graff accelerator AIFIRA (CENBG-France). The $^4He^+$ ions produced, impinged the sample surface at grazing incidence and the hydrogen atoms were collected through a filter (in order to stop He ions). The spectra were processed using SIMRA software. SIMS and ERDA results concerning hydrogen will be discussed in Section 4.2.

3. Results

Typical quantified SIMS depth profiles inside silica thin films deposited on glass are presented on Fig. 2, before and after thermal treatment.

As shown on Fig. 2a and 2c, deposition of silica thin film with our PVD protocol allows us to obtain pure and aluminum-doped silica layers without contamination by the various oxides contained in the glass substrate. Nevertheless, after annealing for one hour at 650°C pure or alumina-doped silica layers (Figs. 2b and 2d), we observe the migration of sodium and potassium from the glass substrate to the silica layer. On the other hand, alkaline-earth elements such as calcium and magnesium are not measured in significant amounts. Interestingly, the concentration of alkali oxides (both Na_2O and K_2O) after thermal treatment is substantially higher for an Al_2O_3-doped silica layer (Fig. 2d) than for a pure silica layer (Fig 2b).

In order to study the relationship between aluminum doping and alkali migration, we extracted the average value of the Na_2O and K_2O content (averaged over a central zone in order to avoid SIMS artifacts at interfaces) in doped and pure silica layers. Na_2O and K_2O contents are plotted respectively in Fig. 3a and Fig. 3b as a function of Al_2O_3 content, for different annealing durations at 650°C. We observe a clear affine relation between Al_2O_3 and alkali oxides concentrations (mol %), with a best least-square fit given by:

$$C_{Na_2O} = 1.47\, C_{Al_2O_3} + 0.22 \qquad (1)$$

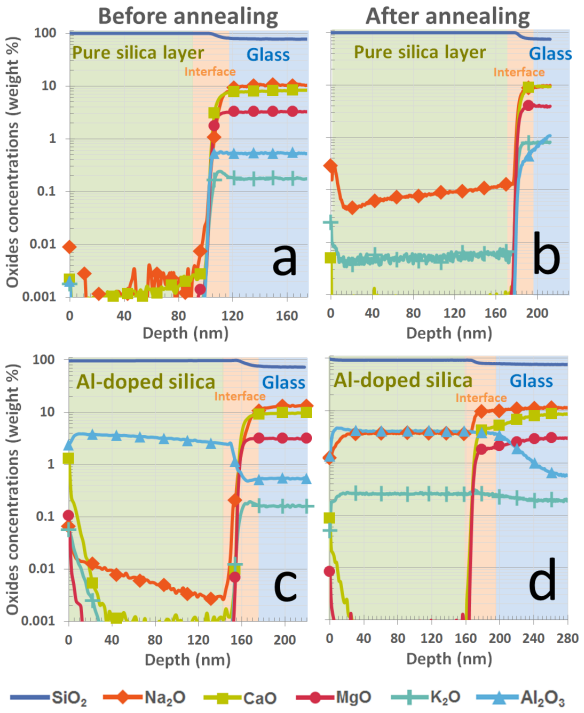

Figure 2: SIMS profiles of silica thin films deposited on glass: a- pure silica layer before annealing, b- pure silica layer after 1h-annealing at 650°C, c- 4-wt% Al_2O_3-doped silica layer before annealing, d- 4-wt% Al_2O_3-doped silica layer after 1h-annealing at 650°C.

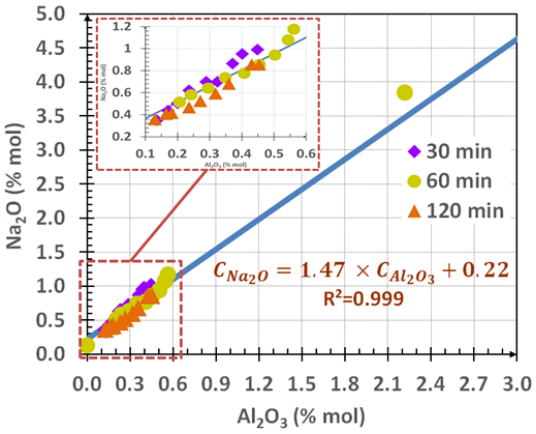

(a)

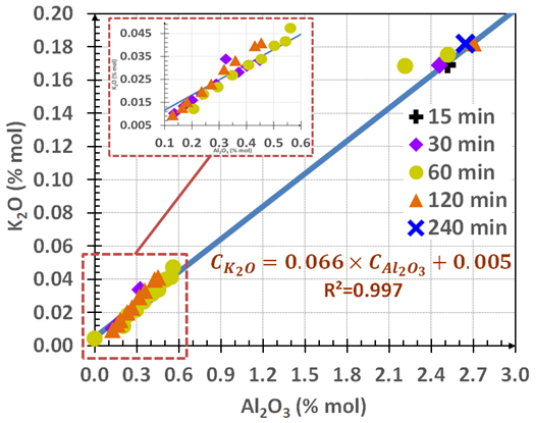

(b)

Figure 3: Na_2O content (a) and K_2O content (b) in silica layers after annealing at 650°C for different Al_2O_3 contents and annealing durations.

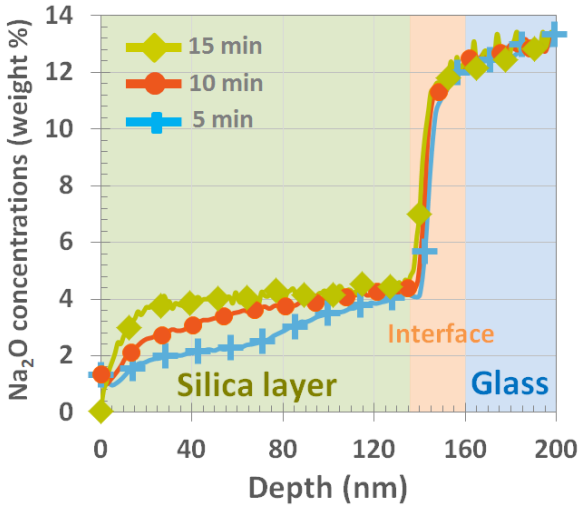

Figure 4: Na_2O SIMS profiles after diffusion in silica layers for short annealing durations at 650°C, for a 4-wt% Al_2O_3-doping of the silica layer.

$$C_{\mathrm{K_2O}} = 0.066\, C_{\mathrm{Al_2O_3}} + 0.005 \qquad (2)$$

The agreement between experimental data and the affine law is as good for both alkali species. However, the K_2O content is very low (always $<$ 0.2 mol %), while the Na_2O content is larger than the Al_2O_3 content, with ∼1.5 times more sodium atoms than aluminum atoms in silica after the thermal treatment at 650°C. Note that the atomic ratio between sodium and potassium is ∼25, while it is 200 in the substrate.

Fig. 3 also shows that, for a given aluminum content, Na_2O and K_2O concentrations saturate after an annealing time of about 15 minutes. For shorter annealing durations, Fig. 4 shows that the sodium concentration increases gradually from the interface with glass to the interface with air. After 15 minutes at 650°C, a uniform sodium concentration profile is observed throughout the layer.

At longer times, the migration of alkali is followed by a dissolution of the silica layer into the substrate, as shown in Fig. 5, where silica profiles are plotted for annealing durations from 15 to 240 minutes. The interface between the silica layer and the glass is marked by a sharp drop of the silica content. The interface shifts gradually from its initial position (green dotted line, which is detected as the position of the Sn^+ peak), toward the upper surface of the film. This shift denotes a dissolution of the silica layer, due to interdiffusion between the high-silica layer and the substrate with a lower sil-

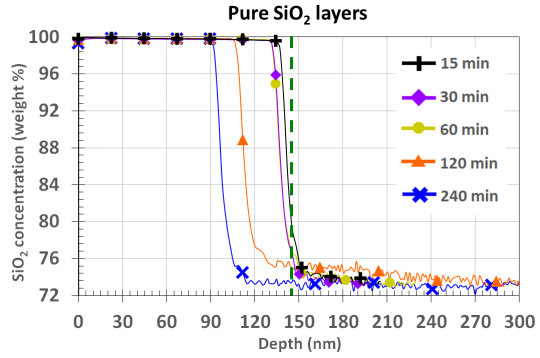

(a)

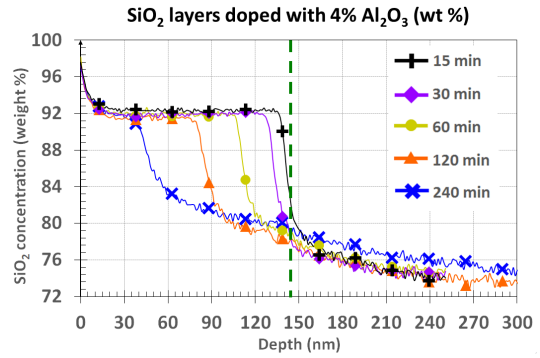

(b)

Figure 5: SiO_2 SIMS profiles of (a) a 150 nm pure silica thin film, and (b) a 150 nm Al_2O_3-doped silica thin film for various annealing durations at 650°C. Interface before annealing (vertical green dotted line) is followed by the maximal value of the Sn^+ peak during SIMS analysis

ica content. For pure silica layers (with 0.2 mol % of Na_2O), the interface is simply translated (see Fig. 5b), as for the dissolution of a mineral. For the 4-wt% Al_2O_3-doped silica layer, the interface remains very sharp on the silica layer side, while it becomes broader on the substrate side, indicating a more pronounced interdiffusion between substrate and layer. Also note that the dissolution is faster for the doped layer than for the pure-silica layer, since the distance between the initial and the new interface grows approximatively twice faster for the Al-doped layer.

This slow process of dissolution of the silica thin film into the glass substrate and its dependence on the aluminum-doping of the layer will be addressed in greater details elsewhere. In the following section, we focus the discussion on the effect of aluminum-doping on the migration of alkali ions from the glass substrate to the silica layer.

4. Discussion

4.1. Mechanism of alkali migration

Our experiments at 650°C demonstrate that alkali ions such as Na^+ and K^+ diffuse from glass to silica thin films. As shown in Figs. 3 and 4, alkali ions concentrations are already equilibrated in silica layers after a few minutes at 650°C independently of the Al_2O_3 content, so that the diffusion length is larger than the 150-nm-width of the silica layer. Previous studies of sodium diffusion in bulk silica glass found diffusivities between 3.10^{-15} and 3.10^{-11} $m^2.s^{-1}$ [2, 38, 39, 40]. The discrepancy between diffusivity values in different experiments was attributed to the variable hydroxyl content of the silica glasses [39], depending on its elaboration process. The presence of H^+ in silica was found to decrease the mobility of Na^+, an illustration of the mixed-alkali effect [41]. Even the smallest diffusivity value obtained in previous studies (3.10^{-15}) gives a diffusion distance of 1 micron in 10 minutes, that is a diffusion length greater than the width of the silica layer. Therefore, constant sodium profiles after 15 minutes at 650°C are consistent with literature values for sodium diffusivity.

For bulk aluminosilicate glasses containing Na_2O and/or K_2O, interdiffusion between melts of differing alkali concentrations is mostly governed by the exchange of alkali ions with SiO_2 [42, 43, 44, 45]. Such exchanges, if present, would result in a variation of the Si/Al ratio before and after sodium migration. However, during alkali-ions migration, we observe that the atomic ratio Si/Al in the silica layer remains constant, as shown in the SiO_2-Al_2O_3-Na_2O phase diagram in Fig. 6 (red dotted arrows). Therefore, the migration of sodium and potassium corresponds to a dilution of the initial composition of the layer, and not to a counter flux of alkali and Si or Al.

Nevertheless, electro-neutrality requires a net flux of another charged species to compensate the charge of additional alkali. Previous studies in barrier layers [2, 19] suggested that a counter-flux of protons enables sodium migration into silica. The influence of water concentration on sodium migration had also been studied in bulk silica [46, 39]. The influence of water is discussed in more details in the next paragraphs.

4.2. Interdiffusion between protons and alkali ions

Water is one of the most common important impurity found in PVD sputtered thin films. It's ori-

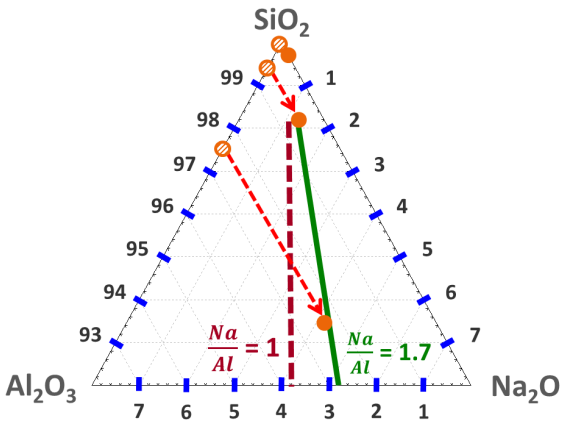

Figure 6: Zoom of the phase diagram in the ternary system SiO_2-Al_2O_3-Na_2O between 92 and 100% SiO_2 in mol %. Empty circles correspond to silica thin films before annealing and filled circles to silica thin films after sodium migration. Red dotted arrows correspond to a constant Si/Al atomic ratio.

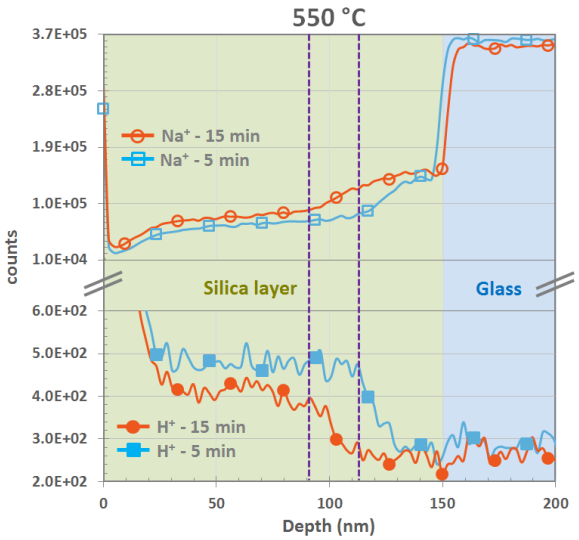

Figure 7: Na^+ and H^+ SIMS profiles after 5 and 15 minutes at 550°C, for a 4-wt% Al_2O_3-doping of the silica layer.

Table 3: Hydrogen content in silica films as measured by ERDA for a pure silica layer or a 2.4-mol% Al_2O_3-doped silica layer. Analyses are performed on samples before and after thermal treatments 30 minutes at 650°C.

H content (mol %)	Before annealing	After annealing
pure silica	0.40 % ≈ 6000 ppm H_2O	< 0.1 %
Al-doped silica	0.38 % ≈ 6000 ppm H_2O	< 0.1 %

gin could be outgassing phenomenon of the deposition chamber walls during the process and surface adsorption during storage due to the porosity of the layers. Table 3 report ERDA measurements that could be performed on two samples (one pure-silica layer and one 2.4-mol% Al_2O_3-doped layer) before and after thermal annealing. They first show that significant hydrogen contents (of the order of half percent) can be found in the deposited silica or aluminum-doped silica thin films. Interestingly, this hydrogen content shows a sharp decrease after thermal treatment.

The loss of H upon annealing is clearly consistent with a scenario of interdiffusion between hydrogens of the layer and alkali ions of the glass substrate. In order to test this hypothesis further we performed SIMS measurements on samples annealed at a lower temperature, T=550°C. The slowing of the dynamics thus allowed us to observe earlier steps of the diffusion process, i.e. before saturation of the alkali content in the film. We show in Fig. 7 SIMS profiles in a 4-wt% Al_2O_3-doped silica thin film of H^+ and Na^+ ions after 5 min. and 15 min. of thermal treatment at 550°C, respectively. Although not quantitative, these profiles show a clear trend: an interdiffusion front of the two species moving from the glass substrate interface toward the surface of the thin film.

4.3. Equilibrium sodium concentration in silica layer

Since alkali concentration is constant after 15 minutes in the silica layers, alkali species are at thermodynamic equilibrium and should have a similar chemical potential in the substrate and in the silica layer. Using the software Factsage® with the FT oxides database and especially the FT oxid-SLAGA module (A-Slag-liq all oxides) developed for silicate systems ([47, 48, 49, 50, 51]), we computed the activity of sodium in the substrate and in the silica layer, for various aluminum and sodium concentrations. In order to stress the crucial effect of the water content in silica films on the alkali diffusion from the glass substrate, we present below results obtained in absence and in presence of water in the films.

The activity of sodium at 650°C as a function of sodium concentration in a dry silica layer is repre-

sented in Fig. 8a, for three different aluminum doping contents. We observe that increasing the aluminum content decreases the activity of sodium, a result that has been obtained experimentally in the literature [52] and that is explained by the smaller sodium content in network-modifying role. A sharp increase of sodium activity occurs when the molar concentration of sodium equates the one of aluminum. Qualitatively, this corresponds to the concentration at which sodium ions charge-compensate all aluminum tetrahedral units. Therefore, the activity of sodium in the layer depends strongly on the aluminum content. In Fig. 8a, the activity of sodium in the glass substrate is represented as a red dotted line.

We define the theoretical sodium equilibrium concentration as the concentration at which chemical potentials are the same in the substrate and the silica layer. The sodium equilibrium concentration is plotted in Fig. 8c (orange line) as a function of aluminum content of the silica layer. We observe an affine (almost linear) relation as in our experiments, but with a different Na/Al atomic ratio: thermodynamic calculations predict a ratio close to one (which amounts to compensating all aluminum tetrahedra), whereas a ratio of 1.5 is observed in our experiments. This means that (in experiments) 1/3 of sodium ions in the silica layer are not charge compensators of aluminum tetrahedra, but network modifiers bound to non-bridging oxygens.

However, it is known [53, 54, 55, 56] that the presence of water modifies the structure of aluminosilicate glasses and melts, hence the activity of sodium in these materials. This strong effect is illustrated in Fig. 8b, where we plotted the activity of sodium in a silica layer as in Fig. 8a, for a layer composition including both the aluminum doping and the presence of water (we arbitrarily chose 6000 ppm of water as measured by ERDA in a Al_2O_3-doped silica layer - 2.4 mol % - cf Table 3, but we found that the value of sodium activity has a very weak dependence with water between 100 ppm to 20000 ppm). Calculations of sodium activities in presence of water are also performed using Factsage ® with the FT oxides database but with the FT oxid-SLAGE module (E-Slag-liq with H2O/OH) which can take into account interactions of water with the silicate network [57, 58]. Comparing Fig. 8a and Fig. 8b shows that: (i) for a pure silica layer, the activity of sodium does not change with or without water, (ii) but for an aluminum-doped silica layer, the activity of sodium changes drastically when water is added. Indeed, the evolution of sodium activity is more gradual in the presence of water, suggesting that water-induced network depolymerization [53, 54] results in a greater diversity of sites for sodium. The sodium equilibrium concentration in the presence of water is plotted in Fig. 8c (violet line). We observe an affine scaling with aluminum content as in water-free layers, but with a greater slope. A least-square fit gives a value of 1.46 for the Na/Al ratio, which is very close to the experimental value (1.47) of Fig. 3a. Therefore, a quantitative prediction of sodium content in the layer can be obtained by balancing sodium activities in substrate and layer, if the presence of some water in the layer is taken into account.

5. Conclusions

In this work we have studied the diffusion processes occurring in silica-based thin films deposited on float glass during thermal treatments above the glass-transition temperature of the glass substrate. Using SIMS analysis, we have quantified the migration of sodium and potassium in silica thin films and shown that their concentration reaches a saturation value after only 15 minutes of annealing at 650°C. The aluminum doping of the silica film has been shown to strongly enhance (with a linear scaling) the diffusion of alkali ions from the glass substrate.

The presence of water in the as-deposited silica films (validated by ERDA measurements) has appeared to be a key element of understanding of this phenomenon. First we could identify an interdiffusion process between the protons of the film and the sodium ions of the glass substrate. Then, taking water into account was shown to drastically modify the thermodynamic activity of sodium in the layer and thus its final equilibrium concentration.

In particular the latter exceeds the aluminum concentration of the thin film. The sodium ions in the aluminum-doped silica layer thus exist not only as charge compensators of the aluminum ions inserted in the silica network but also as network modifiers. As illustrated in Fig. 5, this depolymerization effect of aluminum on the silica network is likely to strongly affect the slower homogenization process (thin film dissolution) occurring at long times and will be addressed in more detailed in a future study.

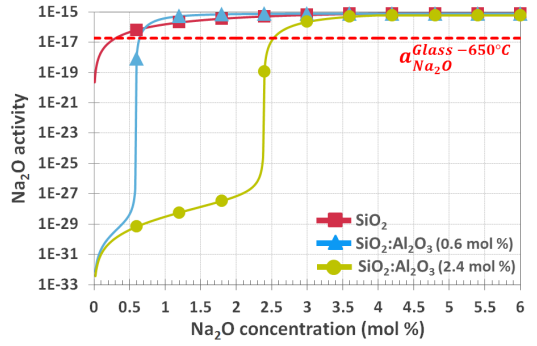

(a)

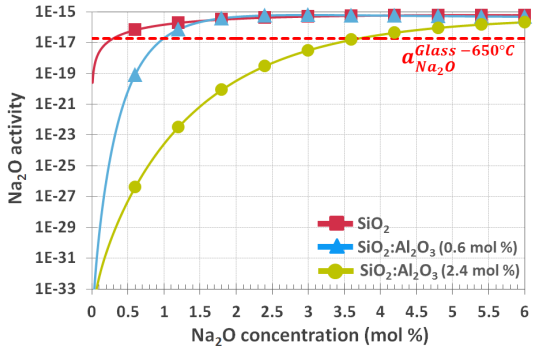

(b)

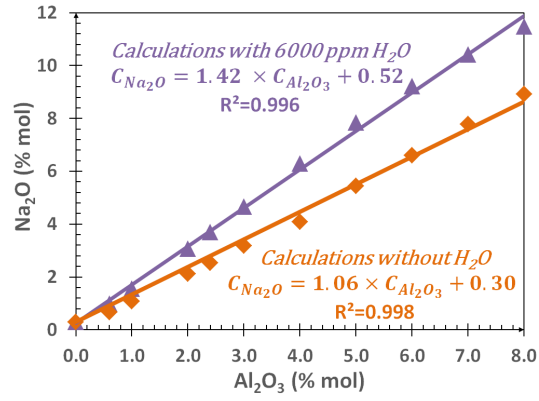

(c)

Figure 8: Energetics of sodium - (a) Na_2O activity in silica layer at 650°C as a function of Na_2O concentration, for different aluminum doping, and for free sodium atoms (i.e., network modifiers and not charge compensators). Calculations are made with Factsage® software, using the FT oxides database. The red dotted line marks the value of Na_2O activity at 650°C in the float glass substrate. (b) Same as (a), for silica layers containing 6000ppm of water. (c) Equilibrium sodium concentration in the silica layer as a function of aluminum doping, for dry layers (orange) and water-containing layers (violet).

Acknowledgments

The authors gratefully acknowledge Thierry Crétin, Corinne Papret and Régine Faure for SIMS measurements at Saint-Gobain Recherche in Aubervilliers (France), Biophy Research in Fuveau (France) for XPS analysis and ARCANE-CENBG in Bordeaux (France) for ERDA analysis. The authors also acknowledge the experimental help of Raphaël Danguillaume, Anne Lelarge, Benoît Louis and Jean-Paul Rousseau, as well as enlightening discussions with Corinne Claireaux and Mike Toplis.

References

[1] S. Ishizuka, A. Yamada, P. J. Fons, H. Shibata, S. Niki, Interfacial alkali diffusion control in chalcopyrite thin-film solar cells, ACS Appl. Mater. Inter. 6 (16) (2014) 14123–30. doi:10.1021/am503480m.

[2] N. Janke, O. Grassme, R. Weimann, Alkali ion migration control from flat glass substrates, Glass Sci. Tech. 73 (2000) 143–155.

[3] J. H. Scofield, S. Asher, D. Albin, J. Tuttle, M. Contreras, D. Niles, R. Reedy, A. Tennant, R. Noufi, Sodium diffusion, selenization, and microstructural effects associated with various molybdenum back contact layers for CIS-based solar cells, in: 24th IEEE Photovoltaic Specialists Conference, Vol. 1, pp. 164–167. doi:10.1109/wcpec.1994.519833.

[4] K. Durose, M. A. Cousins, D. S. Boyle, J. Beier, D. Bonnet, Grain boundaries and impurities in CdTe/CdS solar cells, Thin Solid Films 403-404 (2002) 396–404. doi:10.1016/s0040-6090(01)01518-8.

[5] M. Emziane, K. Durose, D. P. Halliday, N. Romeo, A. Bosio, The distribution of impurities in the interfaces and window layers of thin-film solar cells, J. Appl. Phys. 97 (11) (2005) 114910. doi:10.1063/1.1921344.

[6] L. Kranz, J. Perrenoud, F. Pianezzi, C. Gretener, P. Rossbach, S. Buecheler, A. Tiwari, Effect of sodium on recrystallization and photovoltaic properties of CdTe solar cells, Sol. Energ. Mat. Sol. C. 105 (2012) 213–219. doi:10.1016/j.solmat.2012.06.019.

[7] J. Kulczyk-Malecka, P. J. Kelly, G. West, G. C. B. Clarke, J. A. Ridealgh, Investigations of diffusion behaviour in Al-doped zinc oxide and zinc stannate coatings, Thin Solid Films 520 (5) (2011) 1368–1374. doi:10.1016/j.tsf.2011.08.076.

[8] J. Kulczyk-Malecka, P. J. Kelly, G. West, G. C. B. Clarke, J. A. Ridealgh, Diffusion studies in magnetron sputter deposited silicon nitride films, Surf. Coat. Tech. 255 (2014) 37–42. doi:10.1016/j.surfcoat.2013.11.027.

[9] J.-M. Lee, B.-H. Choi, M.-J. Ji, Y.-T. An, J.-H. Park, J.-H. Kwon, B.-K. Ju, Effect of barrier layers on the properties of indium tin oxide thin films on soda lime glass substrates, Thin Solid Films 517 (2009) 4074–4077. doi:10.1016/j.tsf.2009.01.149.

[10] M. N. Ghazzal, E. Aubry, N. Chaoui, D. Robert, Effect of SiN_x diffusion barrier thickness on the structural properties and photocatalytic activity of TiO_2 films obtained by sol-gel dip coating and reactive magnetron

sputtering, Beilstein J. Nanotech. 6 (2015) 2039–45. doi:10.3762/bjnano.6.207.

[11] F. P. Fehlner, N. J. Binkowski, K. R. Salisbury, L. Button, Alumina barrier layers on LCD glass, J. Non-Cryst. Solids 195 (1996) 89–94. doi:10.1016/0022-3093(95)00473-4.

[12] F. P. Fehlner, Thin films on glass for liquid crystal displays, J. Non-Cryst. Solids 218 (1997) 360–367. doi:10.1016/S0022-3093(97)00243-3.

[13] S. Sonderby, P. L. Popa, J. Lu, B. H. Christensen, K. P. Almtoft, L. P. Nielsen, P. Eklund, Strontium diffusion in magnetron sputtered gadolinia-doped ceria thin film barrier coatings for solid oxide fuel cells, Adv. Energy Mater. 3 (7) (2013) 923–929. doi:10.1002/aenm.201300003.

[14] S. Dreer, P. Wilhartitz, K. Piplits, K. Mayerhofer, J. Foisner, H. Hutter, Quantitative SIMS depth profiling of diffusion barrier gate-oxynitride structures in TFT-LCDs, Anal. Bioanal. Chem. 379 (2004) 599–604. doi:10.1007/s00216-003-2468-y.

[15] J. W. Osenbach, S. S. Voris, Sodium diffusion in plasma-deposited amorphous oxygen-doped silicon nitride (a-SiON:H) films, J. Appl. Phys. 63 (1988) 4494. doi:10.1063/1.340144.

[16] F. Guanghui, D. Jiafeng, P. Donghui, H. Ouli, The migration of alkali ions from glass substrates coated with sol-gel barrier films, J. Non-Cryst. Solids 112 (1989) 454457.

[17] B. M. Davies, K. H. Pannell, S. P. Albright, Diffusion barrier of sol-gel derived silica for sprayed tin oxide film on soda-lime glass, J. Mater. Res. 9 (01) (2011) 226–228. doi:10.1557/jmr.1994.0226.

[18] J. Wolfe, C. Boehmler, J. Hofmann, Method for coating substrates with silicon based compounds - EP0502068B1 (04 1995).

[19] R. J. Araujo, F. P. Fehlner, Sodium redistribution between oxide phases, J. Non-Cryst. Solids 197 (1996) 154–163. doi:10.1016/0022-3093(95)00632-X.

[20] S. K. Lee, J. F. Stebbins, The structure of aluminosilicate glasses: High-resolution ^{17}O and ^{27}Al MAS and 3QMAS NMR study, J. Phys. Chem. B 104 (17) (2000) 4091–4100.

[21] S. K. Lee, J. F. Stebbins, The distribution of sodium ions in aluminosilicate glasses: a high-field Na-23 MAS and 3Q MAS NMR study, Geochim. Cosmochim. Ac. 67 (9) (2003) 1699–1709.

[22] S. K. Lee, J. F. Stebbins, Effects of the degree of polymerization on the structure of sodium silicate and aluminosilicate glasses and melts: An ^{17}O NMR study, Geochim. Cosmochim. Ac. 73 (4) (2009) 1109–1119.

[23] Y. Zhang, H. Ni, Y. Chen, Diffusion data in silicate melts, Rev. Mineral. Geochem. 72 (1) (2010) 311–408.

[24] Y. Liang, Multicomponent diffusion in molten silicates: theory, experiments, and geological applications, Reviews in Mineralogy and Geochemistry 72 (1) (2010) 409–446.

[25] A. M. George, J. F. Stebbins, Dynamics of Na in sodium aluminosilicate glasses and liquids, Phys. Chem. Miner. 23 (8) (1996) 526–534.

[26] J. R. Allwardt, B. T. Poe, J. F. Stebbins, The effect of fictive temperature on Al coordination in high-pressure (10 GPa) sodium aluminosilicate glasses, Am. Mineral. 90 (8-9) (2005) 1453–1457.

[27] Y. Xiang, J. Du, M. M. Smedskjaer, J. C. Mauro, Structure and properties of sodium aluminosilicate glasses from molecular dynamics simulations, J. Chem. Phys. 139 (4) (2013) 044507.

[28] C. Le Losq, D. R. Neuville, P. Florian, G. S. Henderson, D. Massiot, The role of Al^{3+} on rheology and structural changes in sodium silicate and aluminosilicate glasses and melts, Geochim. Cosmochim. Ac. 126 (2014) 495–517. doi:10.1016/j.gca.2013.11.010.

[29] M. J. Toplis, D. B. Dingwell, T. Lenci, Peraluminous viscosity maxima in Na_2O-Al_2O_3-SiO_2 liquids: The role of triclusters in tectosilicate melts, Geochim. Cosmochim. Ac. 61 (13) (1997) 2605–2612.

[30] J. L. Pouchou, F. Pichoir, Analyse d'échantillons stratifiés à la microsonde électronique, Le Journal de Physique Colloques 45 (C2) (1984) 47–50. doi:10.1051/jphyscol:1984212.

[31] Z. Wang, K. Jin, Y. Zhang, F. Wang, Z. Zhu, ToF-SIMS depth profiling of insulating samples, interlaced mode or non-interlaced mode?, Surf. Interface Anal. 46 (S1) (2014) 257–260. doi:10.1002/sia.5419.

[32] Y. Yamamoto, N. Shimodaira, SIMS depth profile analysis of sodium in silicon dioxide, Appl. Surf. Sci. 255 (4) (2008) 860–862. doi:10.1016/j.apsusc.2008.05.069.

[33] S. Krivec, T. Detzel, M. Buchmayr, H. Hutter, On the temperature dependence of Na migration in thin SiO_2 films during ToF-SIMS $O_2{}^+$ depth profiling, Appl. Surf. Sci. 257 (1) (2010) 25–32. doi:10.1016/j.apsusc.2010.06.019.

[34] B. Saha, P. Chakraborty, $MCs_n{}^+$-SIMS: An innovative approach for direct compositional analysis of materials without standards, Energy Proced. 41 (2013) 80–109. doi:10.1016/j.egypro.2013.09.009.

[35] U. Hoffmann, G. Heide, G. H. Frischat, Reactions between solgel coatings and some technical glass substrates during consolidation, Journal of Non-Crystalline Solids 351 (43-45) (2005) 3562–3569. doi:10.1016/j.jnoncrysol.2005.08.032.

[36] G. Heide, C. Muller-Fildebrandt, D. Moseler, G. Frischat, W. Meisel, A. Maldener, A. Zouine-Thimm, F. Rauch, Tin in float glass: A diffusion-reaction model based on surface analysis explains the tin hump, Glass Science and Technology - Glastechnische Berichte 73 (2000) 321–330.

[37] U. Breuer, H. Holzbrecher, M. Gastel, J. S. Becker, H.-J. Dietze, Comparative studies of MCs^+-SIMS and e^--beam SNMS for quantitative analysis of bulk materials and layered structures, Fresen. J. Anal. Chem. 353 (3) (1995) 372–377. doi:10.1007/bf00322072.

[38] G. H. Frischat, Sodium diffusion in SiO_2 glass, J. Am. Ceramic Soc. 51 (9) (1968) 528–530.

[39] L. Tian, R. Dieckmann, C.-Y. Hui, Y.-Y. Lin, J. G. Couillard, Effect of water incorporation on the diffusion of sodium in type I silica glass, J. Non-Cryst. Solids 286 (3) (2001) 146–161.

[40] L. Tian, R. Dieckmann, Incorporation of water into glasses and its influence on the diffusion of cations, including the creation of diffusion barriers, J. Non-Cryst. Solids 352 (6) (2006) 679–689.

[41] J. Isard, The mixed alkali effect in glass, J. Non-Cryst. Solids 1 (3) (1969) 235–261.

[42] S. Chakraborty, D. B. Dingwell, D. C. Rubie, Multicomponent diffusion in ternary silicate melts in the system K_2O-Al_2O_3-SiO_2: I. experimental measurements, Geochim. Cosmochim. Ac. 59 (2) (1995) 255–264. doi:10.1016/0016-7037(94)00283-r.

[43] S. Chakraborty, D. B. Dingwell, D. C. Rubie, Multicom-

ponent diffusion in ternary silicate melts in the system K_2O-Al_2O_3-SiO_2: II. mechanisms, systematics, and geological applications, Geochim. Cosmochim. Ac. 59 (2) (1995) 265–277. doi:10.1016/0016-7037(95)00284-7.

[44] J. E. Mungall, C. Romano, D. B. Dingwell, Multicomponent diffusion in the molten system K_2O-Na_2O-Al_2O_3-SiO_2-H_2O, Am. Mineral. 83 (1998) 685–699. doi:10.2138/am-1998-7-802.

[45] C. Guo, Y. Zhang, Multicomponent diffusion in silicate melts: SiO_2-TiO_2-Al_2O_3-MgO-CaO-Na_2O-K_2O system, Geochim. Cosmochim. Ac. 195 (2016) 126–141.

[46] J. Mecha, J. Steinmann, et al., Mobility of sodium ions in silica glass of different OH content, J. Am. Ceramic Soc. 62 (7-8) (1979) 343–346.

[47] C. W. Bale, P. Chartrand, S. A. Degterov, G. Eriksson, K. Hack, R. Ben Mahfoud, J. Melanon, A. D. Pelton, S. Petersen, Factsage thermochemical software and databases, Calphad 26 (2) (2002) 189–228. doi:10.1016/s0364-5916(02)00035-4.

[48] C. W. Bale, E. Blisle, P. Chartrand, S. A. Decterov, G. Eriksson, K. Hack, I. H. Jung, Y. B. Kang, J. Melanon, A. D. Pelton, C. Robelin, S. Petersen, Factsage thermochemical software and databases recent developments, Calphad 33 (2) (2009) 295–311. doi:10.1016/j.calphad.2008.09.009.

[49] G. Eriksson, A. Pelton, Critical evaluation and optimization of the thermodynamic properties and phase diagrams of the CaO-Al_2O_3, Al_2O_3-SiO_2 and CaO-Al_2O_3-SiO_2 systems, Metall. Trans. 24B (1993) 807–816.

[50] G. Eriksson, P. Wu, A. Pelton, Critical evaluation and optimization of the thermodynamic properties and phase diagrams of the MgO-Al_2O_3, MnO-Al_2O_3, FeO-Al_2O_3, Na_2O-Al_2O_3 and K_2O-Al_2O_3 systems, Calphad Journal 17 (1993) 189–206.

[51] P. Wu, G. Eriksson, A. Pelton, Critical evaluation and optimization of the thermodynamic properties and phase diagrams of the Na_2O-SiO_2 and K_2O-SiO_2 systems, J. Am. Ceram. Soc. 76 (1993) 2059–2064.

[52] S. Abdelouhab, R. Podor, C. Rapin, M. Toplis, P. Berthod, M. Vilasi, Determination of Na_2O activities in silicate melts by EMF measurements, J. Non-Cryst. Solids 354 (26) (2008) 3001–3011.

[53] Q. Zeng, H. Nekvasil, C. P. Grey, In support of a depolymerization model for water in sodium aluminosilicate glasses:: Information from NMR spectroscopy, Geochim. Cosmochim. Ac. 64 (5) (2000) 883–896.

[54] E. Robert, A. Whittington, F. Fayon, M. Pichavant, D. Massiot, Structural characterization of water-bearing silicate and aluminosilicate glasses by high-resolution solid-state NMR, Chem. Geol. 174 (1) (2001) 291–305.

[55] X. Xue, M. Kanzaki, Structure of hydrous aluminosilicate glasses along the diopside–anorthite join: A comprehensive one-and two-dimensional ^{1}H and ^{27}Al NMR study, Geochim. Cosmochim. Ac. 72 (9) (2008) 2331–2348.

[56] W. J. Malfait, X. Xue, The nature of hydroxyl groups in aluminosilicate glasses: Quantifying Si–OH and Al–OH abundances along the SiO_2-$NaAlSiO_4$ join by ^{1}H, ^{27}Al-^{1}H and ^{29}Si-^{1}H NMR spectroscopy, Geochim. Cosmochim. Ac. 74 (2) (2010) 719–737.

[57] I.-H. Jung, Thermodynamic modeling of gas solubility in molten Slags (I) - Water, ISIJ Int 46 (2006) 1587–1593.

[58] A. Pelton, Thermodynamic calculation of gas solubilities in oxide melts and glasses, Glastechnische Berichte 72 (1999) 214–226.